JOURNAL OF MATERIALS SCIENCE 22 (1987) 3148–3160

Structure and chemistry of fibre–matrix interfaces in silicon carbide fibre-reinforced glass–ceramic composites: an electron microscopy study

R. F. COOPER*, K. CHYUNG
Corning Glass Works, Research and Development Division, Corning, New York 14831, USA

Silicon carbide continuous fibre-reinforced glass and glass–ceramic matrix composites showing high strength and fracture toughness have been studied using thin-foil transmission electron microscopy and scanning transmission electron microscopy (AEM). The outstanding mechanical behaviour of these materials is directly correlated with the formation of a cryptocrystalline carbon (graphite) reaction-layer interface between the fibres and the matrix. A solid-state reaction involving relatively rapid diffusion of silicon and oxygen from fibre to matrix correlates well with the experimental observations. Silica activity in the glass–ceramic matrix is suggested to play a primary role in the ability to control the chemical reaction which creates the graphitic interface. AEM results are used to comment upon a possible mechanism for the high-temperature embrittlement behaviour noted for these materials when they undergo rupture in an aerobic environment.

1. Introduction

In pursuit of structural refractory materials which have a high fracture toughness (and consequently high reliability), a substantial research effort has been forwarded towards the development of continuous fibre-reinforced composites which employ refractory ceramic fibres embedded in a glass, glass–ceramic or ceramic matrix. One approach which has yielded much promise has been the use of polymer-melt spun, amorphous silicon carbide fibres (Nicalon®; Nippon Carbon Co.) as a reinforcement agent [1–3]; the Corning effort has successfully created surprisingly tough (K_{Ic} = 10 to 20 MN m$^{-3/2}$) and strong (MOR = 700 to 800 MPa) composite materials employing matrices of Corning Code 1723 glass and lithium–aluminosilicate (LAS), barium–magnesium–aluminosilicate (BMAS) and calcium–aluminosilicate (CAS) glass–ceramics [3]. The achievement of high fracture toughness in these brittle–brittle composite materials requires both strain tolerance to fracture and fibre pull-out at rupture, thus producing a "graceful" failure; one needs to develop, therefore, a fibre–matrix interface which is characterized both by some inherent resiliency and some inherent strength. The strength criterion is a delicate one; the interface must be strong enough to allow load transfer from the matrix to the relatively stronger, stiffer fibre and yet not overly strong, lest fibre pull-out at failure be prohibited and the composite display the brittle behaviour of normal monolithic ceramic materials.

For a given matrix composition, the creation of a final composite having both high strength and high toughness is critically dependent upon the thermal and mechanical history during fabrication. This history will have two primary effects; first, temperature and stress dictate the rheology of the matrix and, therefore, the rate of matrix deformation and consequent consolidation of the composite and, second, the thermal history dictates the kinetics of any solid-state reaction which may occur between the silicate matrix and carbide fibres forming the critical interfacial bond.

This paper outlines an experimental/observational study performed on composites of Code 1723 glass and CAS and LAS glass–ceramic matrices with continuous SiC fibres, to determine the nature (structure and chemistry) of the fibre–matrix interface which allows high-fracture toughness behaviour. The tools employed in this study are high-resolution transmission electron microscopy (HRTEM) and analytical, scanning transmission electron microscopy (AEM, STEM); in both cases, thin foils of real composites were imaged and analysed. Because the SiC fibre composites display severe embrittlement when deformed or fractured at high temperatures in an aerobic environment [3], these microscopy studies were extended to include the interfacial analysis of thin foils which were consequently annealed at high temperatures in air.

2. Experimental approach

2.1. As-pressed composites

A suite of SiC–glass and SiC–glass–ceramic composites was selected for analysis; a list of the materials

*Present address: Department of Metallurgical and Mineral Engineering, University of Wisconsin–Madison, Madison, WI 53706, USA.

0022–2461/87 $03.00 + .12

TABLE I Characteristics of composites studied

Specimen	Primary crystalline phase	Composite ultimate strength (MPa)	Fracture morphology
Code 1723.a	1723 glass	200	"Brittle"
Code 1723.b	1723 glass	870	"Fibrous"
CAS.a	Anorthite	345	"Fibrous"
CAS.b	Anorthite	995	"Fibrous"
LAS	β-Spodumene	925	"Fibrous"

and their thermal histories and mechanical properties is given in Table I. The Code 1723 glass matrix composites were selected because the gross mechanical property differences between specimens appear to be due only to thermal history; the CAS glass–ceramic matrix composites were selected because of (i) the relative simplicity of this matrix composition (CAS.a is stoichiometric anorthite, $CaAl_2Si_2O_8$) and (ii) the primary mechanical property differences between specimens appear to be related to the addition of small amounts of a fining agent to the composition (CAS.b = CAS.a + 1 wt% As_2O_3). In addition, a matrix composition of β-spodumene (LAS) glass–ceramic was selected for examination because the composite displays good mechanical behaviour.

For each composite, thin-foil TEM specimens were prepared by (i) mechanical grinding and polishing to ~ 15 to 20 μm thickness, (ii) mounting foils (3 mm diameter) between copper washers, and (iii) argon-ion bombardment (at 6 kV) until a small hole was achieved. The morphology of each specimen was parallel to the fibre direction and perpendicular to the consolidation direction (i.e. parallel to the original prepreg plies); each specimen originated from the interior of its respective composite. The completed specimens were then coated with a light film (~ 5 nm) of amorphous carbon by vapour deposition, in order to enhance the electrical conductivity of the specimen so that charging would not occur under the electron beam. Early specimens were sandwiched between two copper TEM washers and charging became a significant problem despite the carbon coating. Later specimens were only mounted on a single washer and the carbon coat applied to the free side of the foil; this procedure worked much better.

The specimens were imaged on either a Siemens 102 HRTEM operating at 125 kV or a Jeol 1200EX TEM operating at 120 kV. The analysis techniques employed included standard bright-field (transmitted beam) imaging, dark-field (diffracted beam) imaging, and high-resolution lattice fringe imaging (a combination of transmitted and diffracted beams simultaneously used to create the image) [4]. The strong and tough composites all contained a reaction layer interface of finite thickness (see Section 3); imaging of the actual thickness and structure of this reaction layer required that the specimens be tilted in the microscope (Fig. 1), a procedure easily accomplished by placing the specimen in the stage such that the fibres were aligned parallel to the primary tilt axis of the microscope.

Chemical analyses and additional imaging were performed on a Jeol 200CX Temscan STEM equipped with a Tracor–Northern energy-dispersive X-ray spectrometer (EDS) and an on-line computer. The detector (solid-state Si[Li]) has a beryllium window which limits the sensitivity of the technique to elements heavier than neon. Chemical spectra were collected for 50 sec at an accelerating voltage of 200 kV and a beam current of 15 μA. Computed chemical analyses from the collected spectra were based on the Cliff–Lorimer standardless ratio technique [5] using ratio factors ("k-factors") determined for this specific instrument by Weathers *et al.* [6]. At 200 kV and 15 μA, the diameter of the analysis volume is expected to be less than 50 nm; the radiation damage spot imaged in STEM after an analysis suggests that this limit is correct.

2.2. Oxidized foils

In an attempt to study the nature of oxidation embrittlement in SiC–glass–ceramic composites, 15 μm thick foils of CAS.b were annealed in air at 600 or 900° C for 20 min and subsequently washer-mounted and argon ion-thinned. These foils were then analysed following the procedure outlined above.

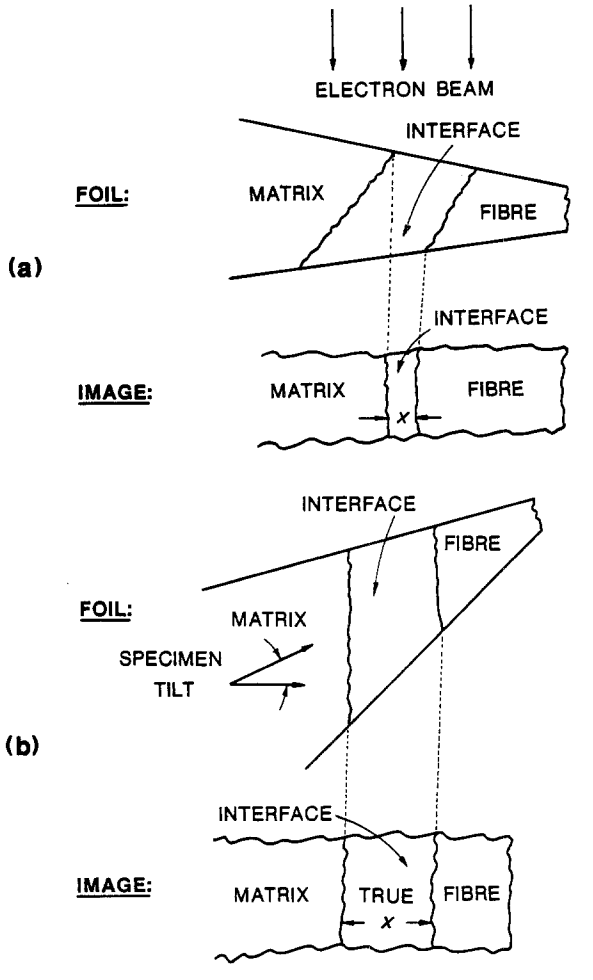

Figure 1 Schematic diagram of TEM foil showing orientation of fibre–matrix interface relative to electron beam: (a) untilted; (b) tilted for "true" view of interface.

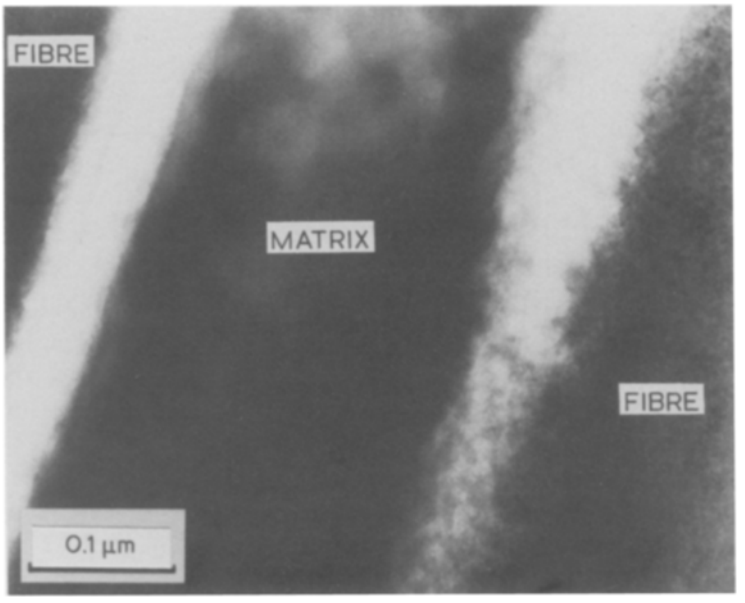

Figure 2 Bright-field TEM micrograph of fibres, matrix and two reaction-layer interfaces in an SiC fibre–1723 glass matrix composite (Code 1723.b).

3. Results

3.1. TEM of composites

Standard bright-field TEM revealed that for each composite displaying a tough, fibrous fracture morphology and relatively high ultimate composite strength, a reaction-layer type fibre–matrix interface could be identified; this layer ranged from 0.02 to 0.2 μm in thickness. The reaction layers display a high electron transmittance; this enhanced transmittance occurs because (i) the layer is composed primarily of light (i.e. low atomic number) elements, and/or (ii) the layer is subject to preferential thinning during specimen preparation (ion bombardment). Fig. 2 shows two such interfaces in the Code 1723.b composite; in this tough material the reaction-layer interface is shown to be constant, ~ 0.08 μm in thickness. In the brittle Code 1723.a composite, no reaction layers were identified; indeed, because of the amorphous nature of both the SiC fibres and the glass matrix, and the high silicon content of each phase, one could not distinguish fibres from matrix in the images of this composite without the reaction layer (the phases could be distinguished, however, from the electron diffraction patterns).

Selected-area diffraction (SAD) apertures are too large to segregate out the interface alone, but SAD patterns could be collected from the fibre separately and from a region containing the interface plus matrix and fibre (imf). Fig. 3 shows SAD patterns from the fibre and the imf area for the LAS matrix composite (similar observations were made on the Code 1723 and CAS composites). From the fibre are collected a series of well-defined rings with diameter ratios (relative to the primary ring) of 1.66 and 1.93 (Fig. 3a);

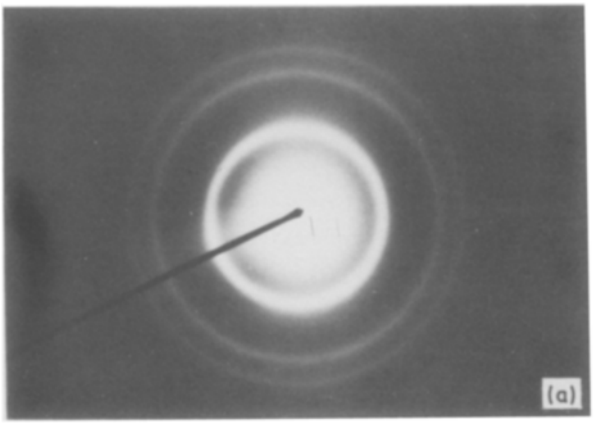

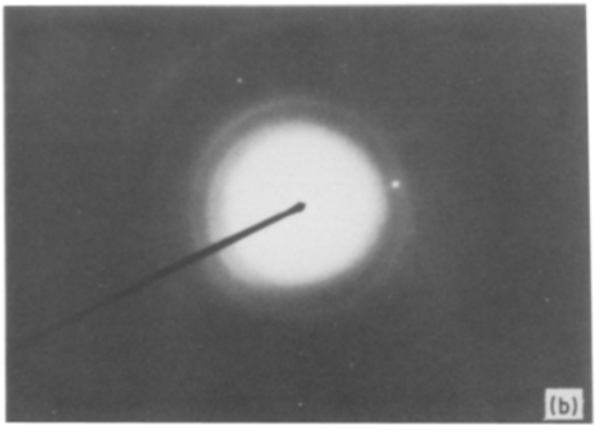

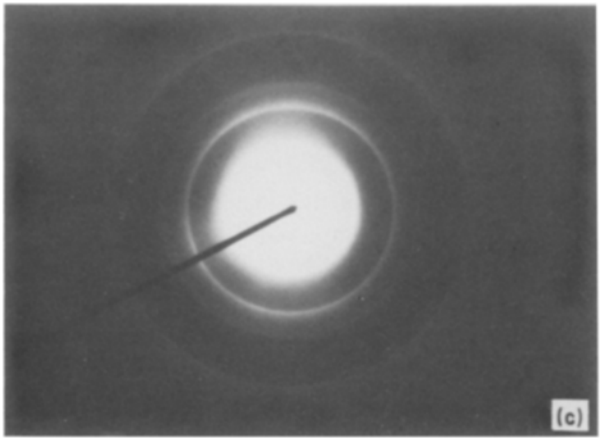

Figure 3 Selected-area diffraction patterns from LAS matrix composite: (a) SiC fibre showing primary and secondary rings of β-SiC; (b) interface-matrix–fibre (imf) region showing primary and secondary rings of β-SiC, primary and secondary rings of graphite, and discrete diffraction spots for β-spodumene; (c) pyrolytic graphite TEM reference standard for comparison with (b).

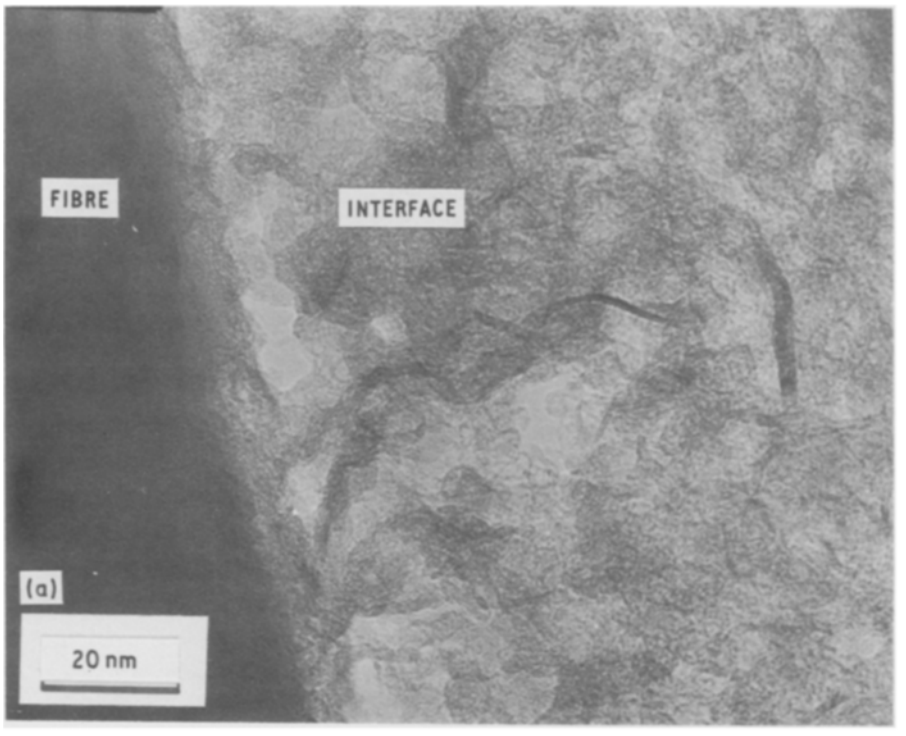

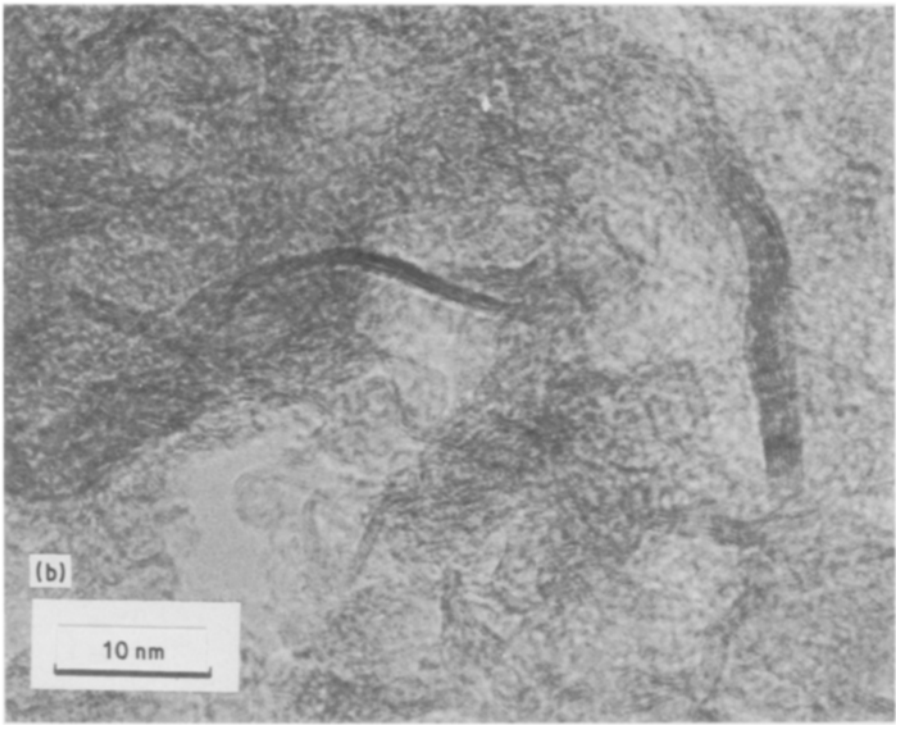

Figure 4 HRTEM lattice fringe image of interface from CAS matrix composite (CAS.b). Fringes show 0.34 nm spacing of (0 0 0 2) planes in graphite.

from an analysis of the pattern one determines that the primary ring corresponds to 0.250 nm and the pattern to beta-SiC (primary ring is (1 1 1) JCPDS diffraction file card No. 1-1119). The imf pattern shows these three primary rings of beta-SiC plus two unique, additional rings with diameter ratios (again, relative to (1 1 1) of beta-SiC) of 0.74 and 1.23 (Fig. 3b). (The discrete diffraction spots originate from the crystalline matrix.) The smallest of the rings corresponds to 0.337 nm; the diameter ratio of these two additional rings is 1.67. While not as sharply imaged as the three beta-SiC rings from the fibre, these two unique rings, which are associated with the interface, are distinct enough to suggest that the interface has a cryptocrystalline nature.

Fig. 4 is a high resolution lattice fringe image from an interface in the CAS.b composite and shows that the interface is mainly comprised of crystallites having a 0.34 nm primary lattice spacing; this lattice spacing and the general morphology of the crystallites correspond to graphite [(0 0 0 2) lattice spacing of 0.336 nm]. The electron diffraction ring pattern with radius ratio 1.67 additionally corresponds to this polymorph of carbon, with the primary ring corresponding to (0 0 2) (0.337 nm) and the secondary ring to (1 0 $\bar{1}$ 1) (0.202 nm). The carbon-rich nature of the fibre–matrix interface was earlier identified by Brennan [7] using scanning Auger electron microanalysis. To our knowledge, this work is the first to directly image and therefore identify crystalline material as a primary

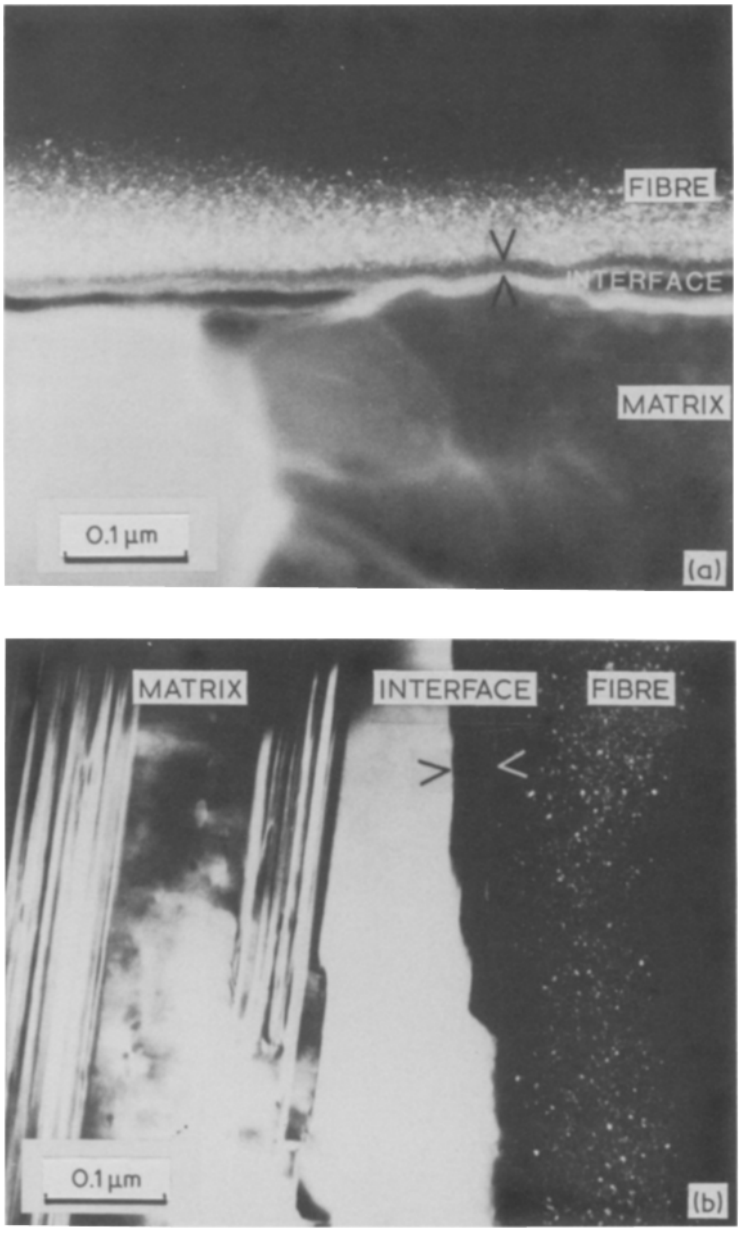

Figure 5 Standard dark-field TEM images of the fibre–matrix interface region in CAS composites (CAS.a): (a) as-pressed, (b) as-pressed plus a 1200° C, 2 h thermal anneal. Micrographs show that thermal annealing increases the thickness of the graphitic interface. Small crystallites (~ 2 nm) of β-SiC are clearly imaged in the fibres. Holes in (a) are artefacts from the ion-thinning process.

constituent of the interface. A crystalline graphite interface has been identified in each of the composites examined in this study with the exception of the brittle, Code 1723.a material; the easy ability to form positive-identification, lattice-fringe images is limited, however, depending upon the thickness of the TEM foil; electron diffraction through many crystallites randomly stacked one upon another gives rise to moiré effects which obliterate the image of any single crystallite [4].

Comparisons between specimens reveal that the formation of the graphite reaction-layer fibre–matrix interface is enhanced with (i) an increase in temperature for a constant time, (ii) an increase in anneal time at a constant, relatively high temperature, and (iii) the addition of a fining agent to the matrix, with time and temperature variables remaining constant. The two Code 1723 glass matrix specimens demonstrate behaviour of the first type, with no interfaces forming in Code 1723.a processed at 950° C and substantial (~ 0.08 μm) interfaces forming in Code 1723.b processed for an identical time but at ~ 1300° C. Fig. 5 illustrates behaviour in the second type; Fig. 5a shows the interface developed in CAS.a (~ 0.02 μm thick), while Fig. 5b shows the interface developed in the same composite when given an additional 1200° C, 2 h anneal at atmospheric pressure (~ 0.06 μm thick). The third behaviour is illustrated by a comparison of CAS.a and CAS.b; the addition of 1 wt % As_2O_3 coarsens the graphitic layer interface from approximately 0.02 μm to approximately 0.1 μm for the same processing conditions (compare Figs 5a and 6a). These three observations support the concept that the reaction layer formation is a dynamic, diffusional process which should be controllable with processing variables and/or matrix composition.

3.2. STEM chemical analyses

Sample STEM EDS analyses for the fibre–matrix interface area of the anorthite (CAS.b) matrix and the β-spodumene (LAS) matrix composites are presented in Table II. The analysis points correspond to the numbered points shown in the bright-field TEM micrographs of Fig. 6; these numbered points actually represent standardized perpendicular distances away from the graphitic interface for those analyses which

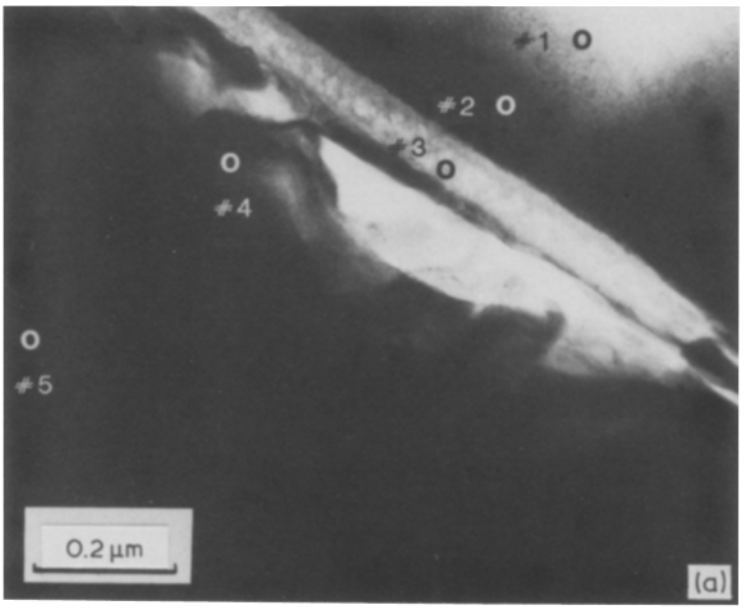

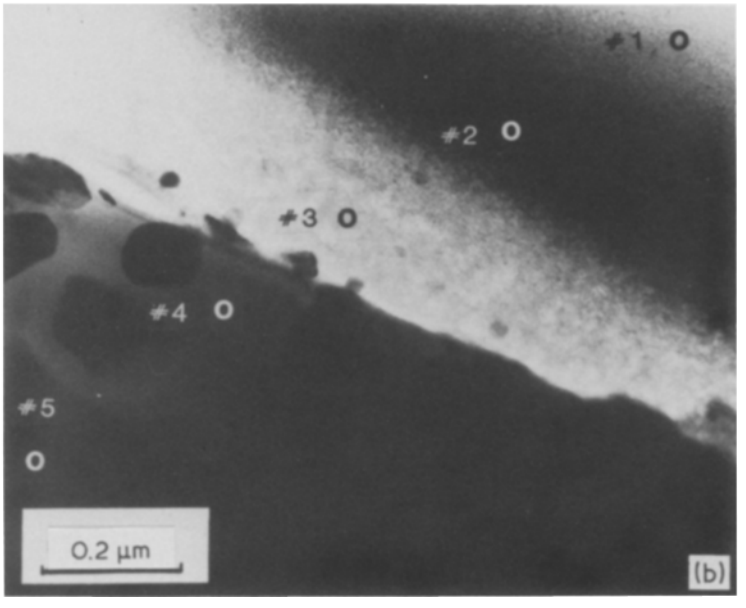

Figure 6 Standard bright-field TEM images showing STEM analysis points corresponding the analyses in Table II. (a) CAS.b matrix composite; (b) LAS matrix composite.

TABLE II STEM analyses of composite interface area

Element	Fibre (Point 1)		Fibre near interface (Point 2)		Interface (Point 3)		Matrix near interface (Point 4)		Matrix (Point 5)		Stiochiomeric anorthite, Cation (%)
	MRC*	Cation (%)	MRC	Cation (%)	MRC	Cation (%)	MRC	Cation (%)	MRC	Cation (%)	
CAS.b (Fig. 5a)											
Si	7912	95.51 ± 3.37†	6605	87.36 ± 0.96	662	53.33 ± 0.39	2942	62.61 ± 2.76	7807	39.49 ± 4.00	40
Al	120	2.60 ± 1.80	448	7.83 ± 0.88	194	20.21 ± 2.78	789	21.63 ± 1.27	6232	40.05 ± 2.70	40
Ca	134	1.29 ± 0.71	312	2.42 ± 0.65	153	7.65 ± 1.07	601	8.00 ± 2.42	6480	19.84 ± 2.16	20
Na	–	–	33	2.24 ± 0.95	36	13.67 ± 0.30	42	4.54 ± 2.42	19	0.50 ± 0.71	–
Fe	–	–	–	–	121	5.16 ± 1.61	273	3.24 ± 1.17	38	0.12 ± 0.16	–
Total		99.40		99.85		100.02		100.02		100.00	100
LAS (Fig. 5b)											
Si	535	99.70 ± 0.42	377	91.05 ± 2.59	15	100.00 ± 0.00	832	77.39‡	894	58.43‡	
Al	–	–	19	6.12 ± 1.65	–	–	188	22.61	481	40.55	
Ca	–	–	10	1.62 ± 0.78	–	–	–	–	–		
Na	–	–	–	–	–	–	–	–	–	–	
Fe	–	–	5	0.71 ± 1.00	–	–	–	–	19	0.67	
Total		99.70		99.50		100.00		100.00		99.65	

*Mean raw counts.
†Errors denote standard deviation of element analysis for 2 to 4 unique point analyses having the same geometrical relationship (i.e. perpendicular distance) to graphitic interface.
‡Single-point analysis.

include two or more independent observations. Mean raw count (MRC) values are shown in the table in addition to cation percentages; variations in MRC for similar analysis area (such as all Points 1 in Figs 6a, 6b, and 7) relate to specimen thickness, which is primarily determined by the degree of specimen tilting necessary to view the true thickness of the fibre–matrix interface.

Important trends in the data include: (i) the actual quantity of metal cations present in the graphitic interface (as evidenced by the variations of MRC between Points 3 and 2, for example) is very small; (ii) inclusion of calcium and aluminium ions (most likely in the form of oxides) into the fibre is noted for both the systems studied, but is more prevalent for the anorthite matrix system; (iii) the matrix composition immediately adjacent to the graphitic interface is significantly enhanced in silica (cf. Points 4 and 5); and (iv) if the MRC data for silicon at Points 3 are normalized by the respective MRC values for silicon of Points 1 (i.e. 662/7912 = 0.0837 for CAS.b and 15/535 = 0.0280 for LAS), it is suggested that the amount of silicon (most likely in the form of silica) contained in the graphitic interface is up to a factor of three greater in the CAS matrix composite than in the LAS one. In addition, the graphitic interface in the CAS matrix composite seems to collect and retain a substantial quantity of aluminium and calcium ions while the LAS material appears to avoid these elements. While LAS contains niobium carbide precipitates (the dark, blocky grains in Fig. 6b) throughout the matrix, with some notable concentration of the grains near the graphitic interface, EDS spectra did not reveal any niobium cations in the interface or in the fibre of this composite (substantial niobium peaks were observed, of course, when an NbC precipitate was analysed).

3.3. Oxidized foils

The CAS.b foils exposed to 600 and 900° C air for 20 min were indeed embrittled, as illustrated by the fact that most fibre–matrix interfaces were either removed or so preferentially ion-thinned as to be impossible to locate on the final foil; this behaviour was particularly noted for the 900° C foil. Remnant interfaces imaged in the 600° C foil were found to be amorphous in structure, as evidenced by both a lack of contrast change during specimen tilting as well as a lack of notable crystalline structure from HRTEM micrographs (Fig. 7a), and to have an average thickness of 0.03 to 0.05 μm. In some interfaces, small (< 0.01 μm) precipitates were found; a lattice-fringe or moiré fringe (~ 0.5 nm spacing) area in Fig. 6a corresponds to one of these precipitates. STEM analyses for an interfacial area in the 600° C anneal are presented in Table III (corresponding to Fig. 7b). Again, notable amounts of aluminium and calcium ions are noted in the interface; however, in this instance, the normalization of the silicon MRC data (in the manner explained above) indicates the silicon level to be approximately five times greater than that for the as-pressed CAS composite. In addition, the silicon level at a distance of 0.06 μm from the edge of the interface on this matrix side shows a notable increase due to the oxidation (compare Points 4 from Tables II and III).

4. Discussion

4.1. Interface formation and solid-state reaction

When the polymer melt-spun SiC fibres are embedded in a multi-component silicate glass or glass–ceramic, a complex reaction couple is created (Fig. 8). An important driving force for the formation of the graphitic interface is surely related to the nature of the SiC fibres.

While referred to as a silicon carbide fibre, Nicalon® is actually a siliconoxycarbide material; studied by a myriad of analytical techniques including TEM, X-ray diffraction (XRD), secondary-ion mass spectroscopy (SIMS) and photoelectron spectroscopy (ESCA), the fibres have been determined to be amorphous in structure (when the pyrolysis of the fibre precursor is performed at $\leqslant 1250°$ C) and to have a uniform, nominal Si : O : C atomic ratio of 3 : 1 : 4 [8–10]. The excess carbon in the fibres is surprisingly stable; pyrolysis of the fibres at $\geqslant 1300°$ C will create a cryptocrystalline fibre microstructure which consists of < 2.0 nm grains of both β-SiC and graphite [11]. These fibres can therefore be characterized by compositional activities of silicon carbode, silica and carbon, each of which is approximately equal to unity (Fig. 8a).

While analysis of many fibre–matrix interfaces has provided some detailed knowledge of the end state (i.e. the "final" reaction-layer interface), very little information is available on the driving forces and kinetics involved in the formation of the graphitic interface. In addition to the kinetics/driving forces observations noted in these experiments (enhancement of interface formation by composite fabrication at either a higher temperature or for a longer high-temperature anneal time, or by addition of a fining agent to the matrix), other correlations of matrix chemistry to interfacial development (at constant temperature and anneal time) observed at Corning Glass Works include: (i) a high alkali content in the matrix precursor glass causes a violent reaction between the matrix and the fibre with foaming of the composite as the usual result; and (ii) additions of so-called "conditional" oxide glass formers to alkali-containing matrix compositions apparently buffer the violent reaction with the SiC fibres. A specific example of this buffering behaviour is the addition of Nb_2O_5 and/or Ta_2O_5 to a standard LAS composition; these additives form an additional NbC or TaC phase, somewhat localized near the graphitic interface (see Fig. 6b, also Brennan [7]). While it was originally thought that this carbide phase forms a coherent, additional reaction layer around the graphitic interface, the TEM observations of the LAS composites studied here indicate that the layer is hardly coherent; the suppression of the foaming reaction caused by the addition of niobium or tantalum oxides cannot be attributed to a protective carbide layer.

The experimental observations combine to suggest that it is the activity of silica or, more specifically, the gradient in silica activity between fibre and matrix which exercises the primary role in the ability to drive

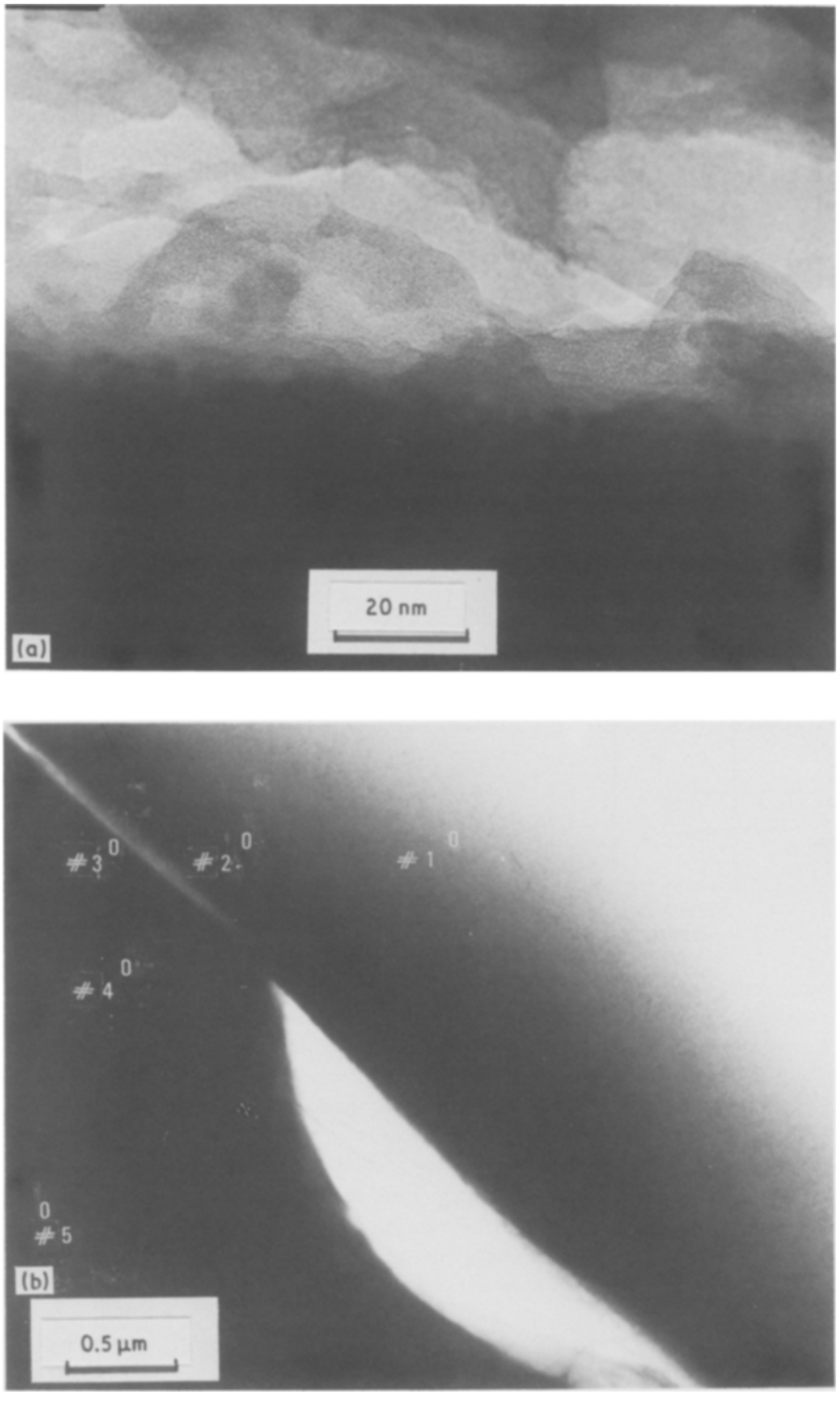

Figure 7 Oxidized CAS.b matrix composite foils: (a) HRTEM lattice fringe image of interface region showing fringes from a precipitate; (b) bright-field image showing STEM analysis points corresponding to the analyses in Table III.

TABLE III STEM analyses of oxidized composite specimen CAS.b; 600° C, 20 min anneal (Fig. 6)

Element	Fibre (Point 1)		Fibre near interface (Point 2)		Interface (Point 3)		Matrix near interface (Point 4)		Matrix (Point 5)	
	MRC*	Cation (%)	MRC	Cation (%)	MRC	Cation (%)	MRC	Cation (%)	MRC	Cation (%)
Si	21160	97.42†	16288	83.04†	8669	73.48 ± 1.15‡	14096	78.21†	9479	40.18 ± 0.47‡
Al	203	1.20	1327	8.74	1377	15.11 ± 1.70	2505	17.93	7462	40.38 ± 0.18
Ca	278	1.38	829	2.61	1085	5.68 ± 0.22	1028	3.51	7587	19.63 ± 0.38
Na	–	–	145	3.45	79	3.11 ± 0.88	–	–	13	0.24 ± 0.34
Fe	–	–	51	0.14	139	0.62 ± 0.04	47	0.14	–	–
K	–	–	572	2.03	340	2.01 ± 0.09	55	0.21	–	–
Total		100.00		100.01		100.01		100.00		100.43

*Mean raw counts.
†Single-point analysis.
‡Errors denote standard deviation of element analysis for 2 to 4 unique point analyses having the same geometrical relationship (i.e. perpendicular distance) to the interface.

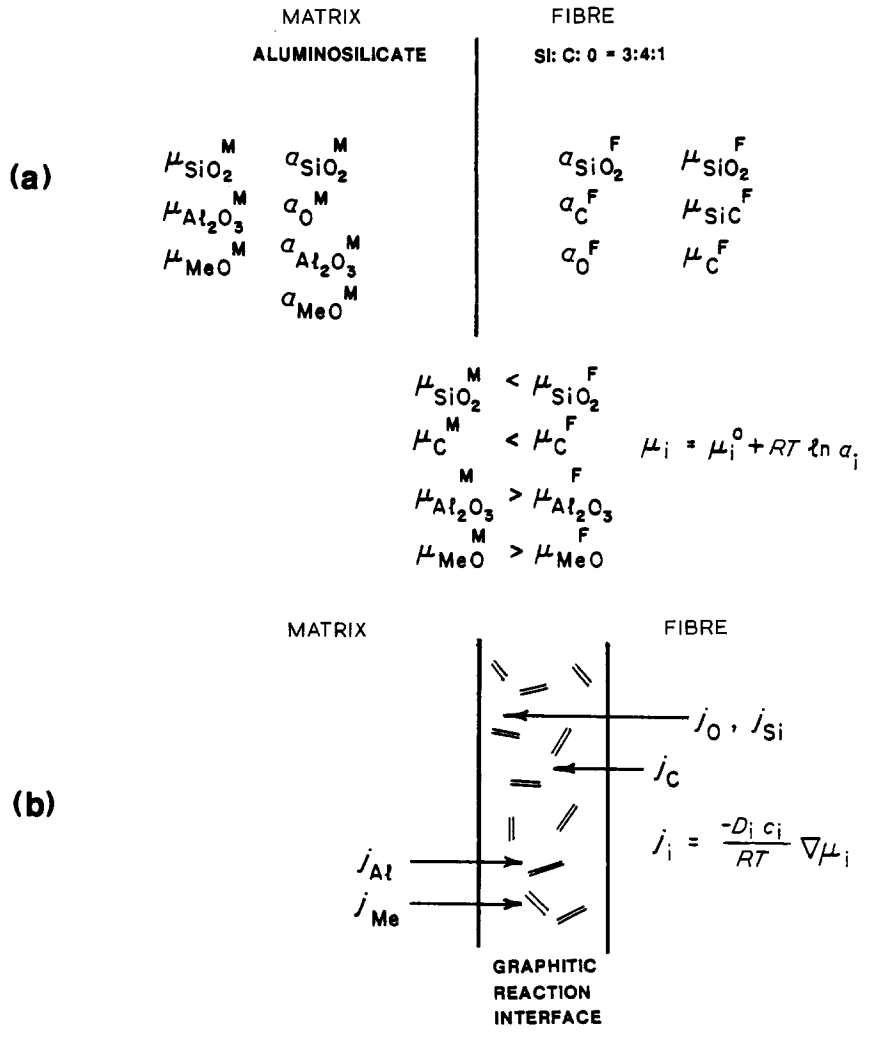

Figure 8 Schematic diagram of the solid-state reaction process (driving forces and molecular transport) proposed for the formation of the graphitic interface. $\mu_i = \mu_i^0 + RT \ln a_i$; $j_i = (-D_i c_i/RT)\nabla\mu_i$. (a) Time $t = 0$; (b) $t > 0$.

and control the solid-state chemical reaction which produces the desired graphitic interface in these composite materials. The presence of a crystalline graphite phase indicates that the chemical equilibrium which characterizes the formation of the interface is

$$SiC(s) + O_2(g) \rightarrow SiO_2(s) + C(s) \quad (1)$$

Applying the law of mass action to Equation 1 gives

$$K_1 = \exp(-\Delta G_1^0/RT) = \frac{a_{SiO_2} a_C}{a_{SiC} a_{O_2}} \quad (2)$$

where K_1 and ΔG_1^0 are the equilibrium constant and change in standard Gibbs free energy for Equation 1, respectively, a_i is the activity of species i, and RT has the usual meaning. In addition to Equation 1, two other equilibria are frequently cited as important in the characterization of oxidation behaviour in silicon carbide:

$$\tfrac{2}{3}SiC(s) + O_2(g) \rightarrow \tfrac{2}{3}SiO_2(s) + \tfrac{2}{3}CO(g) \quad \Delta G_3^0, K_3 \quad (3)$$

which describes "passive" (weight gain) oxidation, and

$$SiC(s) + O_2(g) \rightarrow SiO(g) + CO(g) \quad \Delta G_4^0, K_4 \quad (4)$$

which describes "active" (weight loss) oxidation [12, 13]. Of all the chemical equilibria which describe oxidation of silicon carbide, Equation 1 has the most negative ΔG^0 (up to $T = 1500°$ C, Fig. 9) and, most likely, the most rapid reaction kinetics (for example, Equations 3 and 4 each require the diffusion of a gaseous species away from a reaction interface; this gaseous diffusion is consistently rate-limiting for these reactions). It is not surprising, then, that Equation 1 should characterize the oxidation reaction active within these composites.

From a thermodynamic perspective, the gradient in a_{SiO_2} between fibre and matrix enhances the driving force for Equation 1. In general, the change in Gibbs free energy associated with Equation 1 is

$$\Delta G_1(T) = \Delta G_1^0(T) + RT \ln \left(\frac{a_{SiO_2} a_C}{a_{SiC} a_{O_2}} \right) \quad (5)$$

where $a_C = a_{SiC} = 1$ at the reaction-layer interface. In Equation 5, a_{O_2} will be that of the silicate matrix (which buffers the composite material). This matrix a_{O_2} is that which is "set" in the solid from the atmosphere (partial pressure of oxygen, p_{O_2}) in the melting furnace during the initial preparation of the silicate glass precursor used in an individual composite. Despite the fact that the melting furnace operates in an air environment ($p_{O_2} = 0.21$ atm), the precursor glass never achieves equilibrium with its environment due to sluggish diffusion kinetics; the a_{O_2} of the glass, particularly for those compositions which form composites which have relatively long-term, high-temperature thermochemical stability, will be substantially lower than that of air and most likely will be below the standard-state C : CO buffer (see below). At the fibre–matrix interface, the local a_{O_2} will be buffered

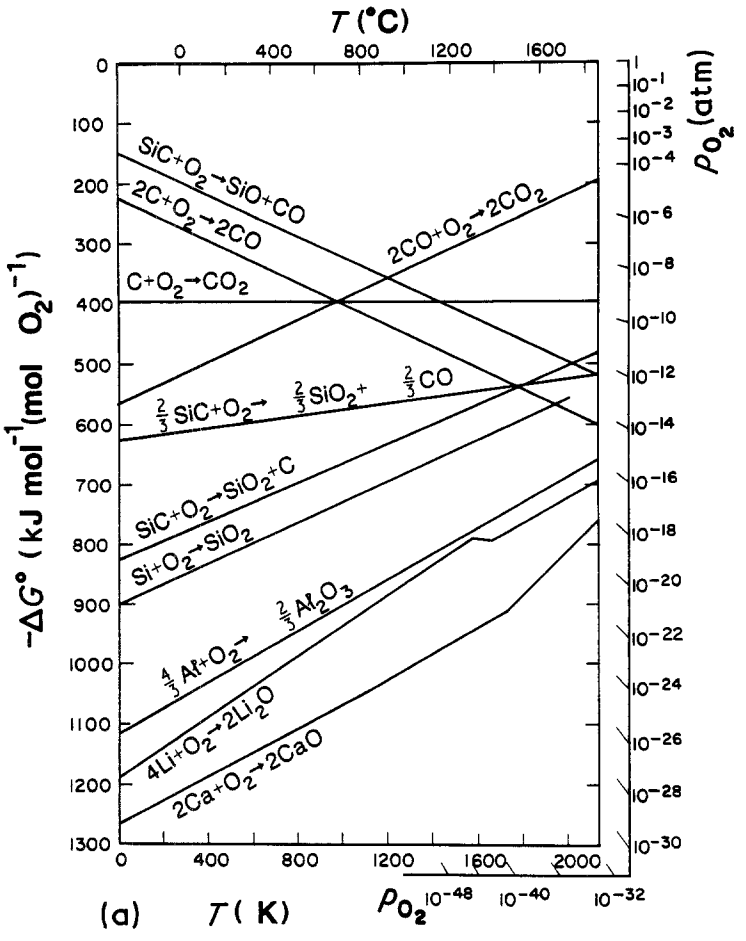

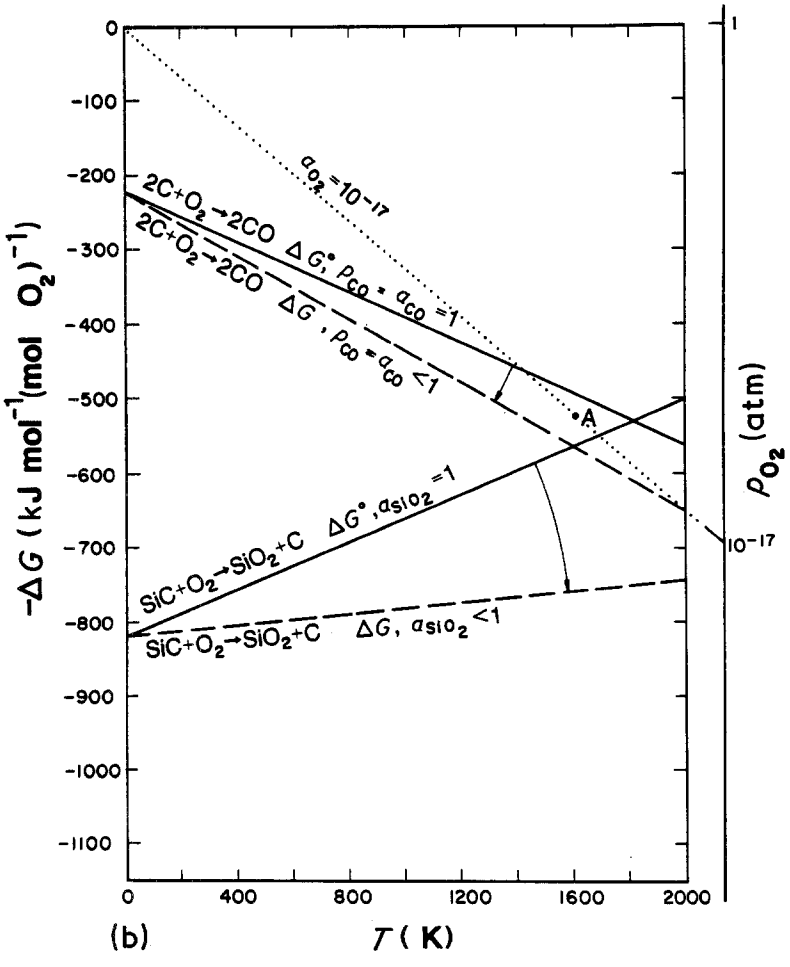

Figure 9 Free energy against temperature (Ellingham) diagrams for the oxidation of metal and carbide species examined in this study: (a) ΔG^0 against T; (b) the mass action law indicates that lowering a_{SiO_2} (accomplished by an increase in matrix basicity away from fused silica) causes clockwise rotation (indicated by arrows) for those SiC oxidation equilibria which include SiO_2 as a reaction product. This behaviour is shown for the reaction of Equation 1. Because basic silicates additionally allow increased solubility of CO, the ΔG^0 line for the C : CO buffer can rotate clockwise as well. On the diagram, a matrix a_{O_2} ($=p_{O_2}$) of 10^{-17} atm at 1600 K (Point A) would promote the formation of a stable graphitic interface if the ΔG^0 lines described all equilibria in the composite. As matrix basicity increases, the reaction of Equation 1 becomes more favourable, but, if the C : CO buffer rotates as well, the a_{O_2} represented at Point A could ultimately exceed the C : CO buffer for the specific composite and cause the composite to foam internally.

to the equilibrium value given in Equation 2. If the activity of silica of the matrix is less than unity, then a_{SiO_2} in Equation 5 will approach the matrix value; in this case, the right-hand term of Equation 5 will be negative, and the ΔG_1 will be still more negative than ΔG_1^0; that is, as a_{SiO_2} of the matrix decreases, the reaction of Equation 5 becomes more favourable (the reaction experiences a greater driving force). Graphically, the ΔG_1 against T linear relationship will pivot clockwise, away from the $\Delta G_1^0(T)$ line (Fig. 9b).

The activity of silica in a silicate glass or ceramic matrix is most markedly affected by the addition of oxide components which serve to make the matrix phase more basic. Acidity/basicity in silicates is characterized by the degree of structural polygonization; acid silicates are characterized by a relatively high density of covalent bonds (i.e. Si–O–Si) and are highly polygonized and quite reducing, while basic silicates are characterized by a relatively high density of ionic bonds and are poorly polygonized and quite oxidizing. From a glass context (though crystalline materials are directly analogous), the addition of network-modifying oxides, such as alkali oxides (an extreme example), to the bulk composition serves to make the glass more basic (i.e. lower the a_{SiO_2}):

$$2Si(O_{1/2})_4 + R_2O \rightarrow 2[Si(O_{1/2})_3O^-] + 2R^+ \quad (6)$$

where $O_{1/2}$ represents an oxygen shared (bridged) between two silicons [14]. In Equation 6, $SiO_{3/2}O^-$ represents a silica tetrahedron which can be ionically bonded to some metal cation (a non-bridging oxygen in the glass context). As matrix basicity increases, a_{SiO_2} decreases and a_{O^-} (the "oxygen ion" activity, represented in Equation 6 by $SiO_{3/2}O^-$) increases. Because an increase in matrix basicity (for a constant a_{O_2} in the matrix) provides a decrease in silica activity, it additionally provides an increase in the driving force, ΔG_1, for the interface-forming reaction (see above); with this increase in driving force, an associated increase in reaction kinetics is also achieved. For the systems cited above, LAS is more basic than CAS, and CAS.b is more basic than CAS.a; the relative reactivity between fibre and matrix noted for these systems is therefore affirmed.

A reasonable conclusion based on the observations cited above is that the graphitic reaction interface forms, and is kinetically rate-limited, by rapid diffusion of oxygen and silicon ions down the silica activity gradient from fibre to matrix. A gradient in carbon activity between fibre and matrix suggests that carbon may diffuse into the matrix as well. The morphology of the reaction-layer interface, whose edge with the silicon carbide fibre is almost always very straight, suggests that the interface surely grows primarily "into" the fibre; any carbon diffusion into the matrix must consequently be very slow. At the same time, diffusion of relatively ionically bonded metal cations (aluminium, calcium, sodium, etc.) can occur from matrix to fibre. The suggested process is schematically depicted in Fig. 8b.

The enhanced oxidation potential of basic silicate matrix compositions is additionally responsible for the foaming noted in LAS matrix composites in which no conditional network-former oxides have been added to buffer the fibre–matrix reactivity. One additional property of basic silicates in an enhanced solubility of carbon oxide gases (CO and CO_2) relative to that in acid silicates [14]; if the solubility of CO in a matrix is significant, the law of mass action indicates that ΔG for the oxidation of carbon may exceed (be more negative than) ΔG^0. Despite the fact that a matrix a_{O_2} may be below the standard-state C:CO buffer, as defined by the ΔG^0 on an Ellingham diagram (Fig. 8), if matrix basicity exceeds a certain amount, the graphite interface will not be stable and foaming caused by release of CO gas will occur. The enhanced solubility of CO in a basic matrix could also cause the ΔG_4 of the active oxidation equation for silicon carbide (Equation 4) to exceed its ΔG_4^0 such that this reaction might prove more favourable than the graphitic interface-forming oxidation equilibria (Equation 1). The addition of conditional network-former oxides to highly basic matrix compositions decreases the matrix basicity and consequently its destructive reactivity.

The discussion to this point has concentrated on solid-state oxidation reactions between silicon carbide and silicates, with no mention of the form of the carbide phase; it is perhaps useful to address the ideas outlined above relative to the Nicalon siliconoxycarbide fibre. Because Nicalon has been characterized as having activities of SiC and C which are approximately unity [11], the graphite which makes up the reaction-layer interface in these composites would therefore consist of that carbon formed by the oxidation of the SiC component of the fibre (by the reaction of Equation 1) *plus* the condensed carbon that is inherently a part of the fibre. The growth rate of the graphite layer for composites made with the Nicalon fibre would therefore appear to be far faster than that seen in composites made with (for example) pure SiC monofilament fibres. In addition, because rapid diffusion paths (like grain boundaries, amorphous films and dislocations) increase the kinetics of solid-state reactions, the amorphous to cryptocrystalline (Fig. 5) state of the Nicalon fibres would also enhance the overall growth rate of the graphite reaction layer over other forms of silicon carbide.

The long-term high-temperature stability of an almost pure carbon interface within a silicate body requires that the a_{O_2} of the matrix remain below the C:CO buffer. If a matrix composition is selected such that its basicity is appropriately limited, and if the a_{O_2} of the matrix is maintained at an appropriately low value during original formation of the matrix in the glass-melting furnace, then internal high-temperature stability of the composite can be maintained. If an internally stable composite is subjected to a high-temperature aerobic environment, the a_{O_2} of the matrix will slowly, through chemical diffusion, climb to achieve equilibrium with the $a_{O_2}(p_{O_2})$ of the environment; foaming of the composite from the surface, advancing inward with time, will be the result. Apart from the mechanical embrittlement problem noted for these materials when fractured in an aerobic environment (see below), the SiC fibre composites will also

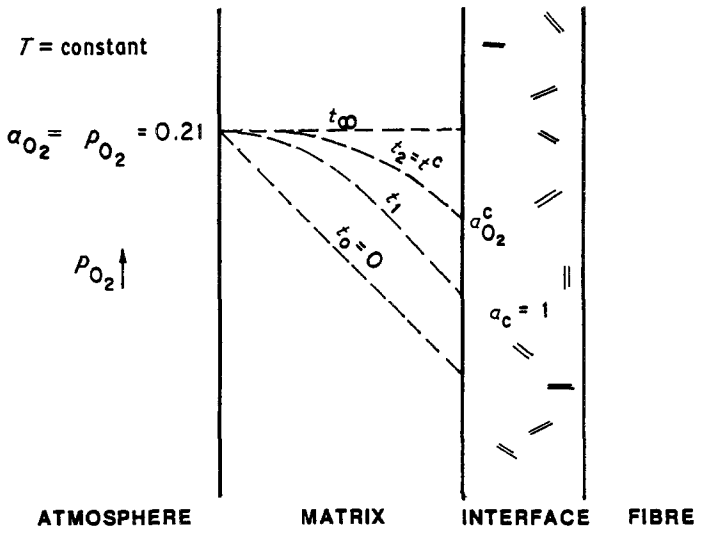

Figure 10 Schematic diagram representing the oxidation process of SiC–silicate composite at a high temperature in air. a_{O_2} at the reaction layer is originally low enough that carbon is stable ($a_C = 1$). A diffusion process will cause the composite to slowly move to equilibrium with the air environment; when a_{O_2} at the graphite layer exceeds some critical value (the C:CO buffer) foaming may occur.

have a kinetic lifetime in air based on thermochemical stability of the graphite interface. This behaviour is schematically shown in Fig. 10.

4.2. Oxidation behaviour on exposure to air

SiC glass and glass–ceramic composites display a pronounced embrittlement when fractured at high temperature in air; the problem is carefully illustrated in the work of Stewart *et al.* [3]. Of curious interest in this phenomenon is the difference in the morphology of the oxygen-embrittled fracture surface between the LAS and CAS matrix composites; embrittled CAS composites display a smooth fracture morphology and a coherent, amorphous bonding between the matrix and the fibres, while the LAS composites display some fibre pull-out and a pronounced ($< 0.5\,\mu m$) gap between the fibres and the matrix. While this mechanical behaviour is complex, it is the structure and chemistry of the graphitic interface which are immediately suggested as primary (though perhaps not unique) causes for the difference in mechanistic behaviour of fracture between the two composites.

The oxidized foils of CAS.b examined in this study indicate that, upon exposure to high-temperature air when the matrix begins to locally microcrack, the graphite in the interface is rapidly oxidized, most likely to CO; this fact is primarily evidenced by the relatively few fibre–matrix interfaces located in a TEM specimen (compared to an as-pressed composite specimen) and the almost total mechanical incoherence – extreme brittleness with little strength – of the oxidized foils. However, in the imaged and chemically analysed fibre–matrix interfaces one discovers a new, amorphous layer which is apparently narrower than the former graphitic interface and exhibits much of the electron transmission of an aluminosilicate glass. A comparison of interfacial composition between the as-pressed CAS and oxidized CAS matrix composites (compare Points 3 in Tables II and III) indicates that the oxidized interface is characterized by a higher silicon content, but the aluminium/calcium cation percentage ratio remains constant. While the STEM used in this study is incapable of analysing carbon or oxygen, it nevertheless appears that the primarily graphitic interface is metamorphosed into a silicate glass upon air pyrolysis, with the metal cation content of this silicate phase determined by the original metal cation content found in the interface. The additional silicon noted in the "new" interface area most likely arises from the passive oxidation of the SiC component in the Nicalon fibres upon removal of the graphitic interface; upon exposure to high-temperature air, silicon carbide will rapidly "sweat" a protective skin of amorphous silica according to the passive oxidation reaction, Equation 3 [9, 12, 13].

An amazing aspect of the oxygen embrittlement phenomenon in the CAS composites is the exceedingly rapid kinetics of carbon removal from the graphitic interface and subsequent replacement of the interface with a new, quite coherent aluminosilicate interface; the gross oxidation embrittlement behaviour during fracture is noted after only about 1 min at 900° C once the matrix microcrack stress is exceeded [3]. This rate of formation of an $\sim 0.03\,\mu m$ reaction layer exceeds by some orders of magnitude the rate of passive oxidation of Nicalon fibres [15]. One possible hypothesis is that it is the silicon, aluminium and calcium ions within the graphitic interface which allow the rapid formation of an oxide layer upon pyrolysis. Referring to the Ellingham free energy diagram shown in Fig. 9a, one sees that while the driving force for oxidation of carbon is large ($\Delta G^0 = -480\,kJ\,mol^{-1}$ at 1200° C), the oxidation driving force for elemental silicon, aluminium and calcium is far greater ($\Delta G^0 = -607$, -795 and $-963\,kJ\,mol^{-1}$, respectively, at 1200° C). If the silicon, aluminium and calcium ions in the interface are not already bonded to oxygen, it is easily imagined that, in the process of oxidizing and vaporizing the carbon, these metal oxides will form at a rate similar to the carbon–oxygen reaction. Later, increases in silica can come from the slower, passive oxidation of the now more exposed Nicalon fibre. It is also important to note that these chemical oxidation processes are exothermic; oxidation of the interface should additionally raise the local temperature, which would enhance the reaction kinetics.

The lack of formation of a coherent interface noted in the LAS composites fractured in air at high temperature coincides well with the model explored above. STEM analysis indicates that these interfaces

are virtually devoid of any metal cations besides silicon (although lithium, which is STEM transparent, may be present; this ion, however, has not been observed in the interface by scanning Auger microanalysis [7]), and the silicon level here is quite low compared to the CAS composite studied. The gap observed between fibres and matrix of the fractured LAS matrix specimens would be expected, of course, if the only process active at the interface was the removal of carbon. It is important to emphasize, however, that the embrittlement is a kinetic problem; the lack of rapid formation of a coherent, amorphous silicate layer between fibre and matrix may therefore solely be related to the fact that the original graphitic interface in the LAS matrix composites often has a greater thickness than those of the CAS matrix materials (compare, for instance, Figs 6a and b).

5. Conclusions

The high fracture toughness and high strength behaviour of SiC fibre-reinforced glass and glass–ceramic matrix composites are directly correlated with the presence of a cryptocrystalline carbon (graphite) reaction layer interface between the matrix and the fibre. The morphology and chemistry of this interface are consistent with the interface having been formed by an SiC oxidation reaction (Equation 1) which is rate-limited by solid-state diffusion of silicon and oxygen down a silica activity gradient from fibre to matrix. Matrix basicity, as it affects both the activity of silica and the oxidation potential of the matrix, is inferred to be a critical factor in the internal thermochemical stability of the composites. STEM analyses indicate that the CAS matrix composites also incorporate aluminium, calcium and silicon in the graphitic layer; LAS matrix composites also incorporate some silicon in the reaction interface, but at lower concentrations than the CAS materials.

The fibre–matrix interfaces in oxidized foils are determined to have a silicate composition, consistent with the metal cation contents incorporated into the original graphitic interface. The high driving force for oxidation of these metal cations may allow the rapid formation of the strong silicate reaction layer that characterizes CAS matrix composites that are fractured in a high-temperature aerobic environment.

Acknowledgements

The microscopy and chemical analyses reported here were performed at the Electron Microscopy Facility of the Materials Science Center at Cornell University; the instruments there are beautifully maintained by the efforts of R. Coles and J. Hunt, who were very helpful in the course of this investigation. We gratefully acknowledge many pleasant, informal discussions with R. Stewart and M. Taylor of Corning Glass Works, D. Kohlstedt and D. Dimos of Cornell University, and E. Hellstrom and Y. Chang of the University of Wisconsin–Madison.

References

1. J. J. BRENNAN and K. M. PREWO, *J. Mater. Sci.* **17** (1982) 1201.
2. *Idem, ibid.* **17** (1982) 2371.
3. R. L. STEWART, K. CHYUNG, M. P. TAYLOR and R. F. COOPER, in "Fracture Mechanics of Ceramics", Vol. 7, edited by R. C. Bradt, A. G. Evans, D. P. H. Hasselman and F. F. Lange (Plenum, New York, 1986) p. 33.
4. P. HIRSCH, A. HOWIE, R. B. NICHOLSON, D. W. PASHLEY and M. J. WHELAN, "Electron Microscopy of Thin Crystals" (Krieger, New York, 1977) p. 563.
5. G. CLIFF and G. W. LORIMER, *J. Micros.* **103** (1975) 203.
6. M. S. WEATHERS, C. A. GOODRICH, J. M. BIRD and J. A. HUNT, *Amer. Mineralogist* (submitted).
7. J. J. BRENNAN, External Report of United Technologies Research Center No. R84-916018-4 (1984).
8. M. P. TAYLOR, Corning Glass Works Internal Report No. R-8810 (1982).
9. T. MAH, N. L. HECHT, D. E. McCULLUM, J. R. HOENIGMAN, H. M. KIM, A. P. KATZ and H. A. LIPSITT, *J. Mater. Sci.* **19** (1984) 1191.
10. G. SIMON and A. R. BUNSELL, *ibid.* **19** (1984) 3658.
11. S. YAJIMA, K. OKAMURA, T. MATSUZAWA, Y. HASEGAWA and T. SHISHIDO, *Nature* **279** (1979) 706.
12. E. A. GULBRANSEN and S. A. JANSSON, *Oxidation Metals* **4** (1972) 181.
13. G. ERVIN, *J. Amer. Ceram. Soc.* **41** (1958) 347.
14. A. PAUL, "Chemistry of Glasses" (Chapman and Hall, London, 1982) p. 176.
15. R. WARREN and C.-H. ANDERSSON, *Composites* **15** (1984) 101.

Received 17 September 1986
and accepted 16 January 1987